Red- and blue-detuned magneto-optical trapping with liquid crystal variable retarders

B. Piest ✉ iD ; V. Vollenkemper iD ; J. Böhm iD ; A. Herbst iD ; E. M. Rasel

Check for updates

View Online   Export Citation   CrossMark

Review of Scientific Instruments

AIP Publishing

Red- and blue-detuned magneto-optical trapping with liquid crystal variable retarders

View Online   Export Citation   CrossMark

B. Piest,[a] (iD) V. Vollenkemper, (iD) J. Böhm, (iD) A. Herbst, (iD) and E. M. Rasel (iD)

AFFILIATIONS

Institut für Quantenoptik, Gottfried Wilhelm Leibniz Universität, Welfengarten 1, 30167 Hannover, Germany

[a]Author to whom correspondence should be addressed: piest@iqo.uni-hannover.de

ABSTRACT

We exploit red- and blue-detuned magneto-optical trapping (MOT) of ^{87}Rb benefitting from a simplified setup and a novel approach based on liquid crystal variable retarders (LCVR). To maintain the trapping forces when switching from a red- to a blue-detuned MOT, the handedness of the circular polarization of the cooling beams needs to be reversed. LCVRs allow fast polarization control and represent compact, simple, and cost-efficient components, which can easily be implemented in existing laser systems. This way, we achieve a blue-detuned type-II MOT for 8.7×10^8 atoms of ^{87}Rb with sub-Doppler temperatures of 44 μK well below the temperatures reached in a conventional ^{87}Rb type-I MOT. The phase space density is increased by more than two orders of magnitude compared to the standard red-detuned type-I MOT. The setup can readily be transferred to any other systems working with ^{87}Rb.

I. INTRODUCTION

Trapped cold atoms with high phase-space densities (PSD) are widely used in a wealth of experiments in atomic, optical, and molecular physics; cold chemistry; and nanophysics. Typical applications range from inertial sensing,[1] optical frequency standards[2] to ultra-sensitive isotope trace analyses[3] or bright sources for ion beams.[4] The most commonly used approach to generate cold atoms is the use of the so-called type-I MOT,[5] although the achievable PSD in conventional magneto-optical trapping (MOTs) is constrained by atom collisions,[6] photon reabsorption,[7] and the lack of sub-Doppler cooling forces in magnetic fields.[8] In contrast to other approaches,[9,10] blue-detuned type-II MOTs address these limitations primarily by enabling sub-Doppler forces even in non-zero magnetic fields.

MOTs can be realized by using either type-I or type-II transitions, which refer to the involved atomic substates of the idealized two-level system. In type-I MOTs, the total angular momentum of the excited state F' is larger compared to that of the ground state F, thus satisfying $F' = F + 1$. Type-II MOTs, in contrast, make use of transitions where $F' = F$ or $F' = F - 1$ (see Fig. 1 for ^{87}Rb), which makes them suitable candidates to realize molecular MOTs.[11–14] When using blue-detuned light fields in a type-II MOT, the sub-Doppler cooling forces are substantially enhanced albeit capturing

and cooling atoms with higher temperatures are not feasible.[15] Thus, to efficiently access the sub-Doppler cooling range, a pre-cooled atom ensemble loaded via a standard type-I MOT is required.[16] Furthermore, either the polarization of the light fields or the sign of the magnetic field gradients has to be reversed when switching between the two MOT types to maintain the position-dependent trapping forces. This switching time limits the capture efficiency of the type-II MOT since the atoms fall and expand freely in between. Due to the inductance of the MOT coils and additional eddy currents in metallic chambers, this timescale is typically above 10 ms.[17–19] On the other hand, reversing the polarization of the MOT beams requires sophisticated optical setups.[15,16]

Here, we demonstrate that liquid crystal variable retarders (LCVRs) can be used to upgrade existing laser systems to allow switching from a conventional red-detuned MOT to a blue-detuned type-II MOT. With this marginally altered setup, we increase the PSD of an ^{87}Rb type-I MOT by more than two orders of magnitude while keeping 84% of the atoms trapped. We also show the feasibility of cooling and trapping of ^{41}K or ^{39}K in a type-II MOT, although no improvement compared to type-I MOTs is observed.

Due to its simplicity, the setup is especially suitable for compact devices such as mobile atom sensors[20,21] or space-borne experiments[22–24] and can easily and cost-efficiently be implemented in existing setups.
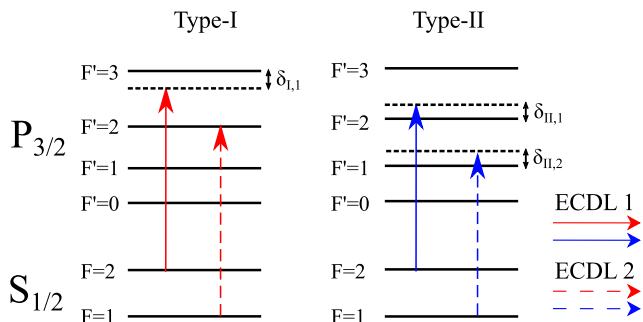
FIG. 1. Frequency detunings used for the type-I and type-II MOTs, respectively. The experimentally determined ideal frequency detunings are $\delta_{I,1} = -11$ MHz, $\delta_{II,1} = 46$ MHz, and $\delta_{II,2} = 22$ MHz. ECDL 1 and ECDL 2 are indicated by solid (dashed) arrows.

II. SETUP

The experimental setup shown in Fig. 2 has initially been designed to operate only type-I ^{87}Rb MOTs. The experimental chamber features a multi-layer atom chip with an integrated U-shaped wire structure, which is housed in a vacuum system. Together with two external Helmholtz coils along the y-direction, this enables the generation of the required magnetic fields in a quadrupole configuration.[25,26] Four collimators are fixed around the vacuum chamber to form the MOT light fields, two of them being reflected on the atom chip surface. The details of the system are described in Piest[23] The laser light is delivered via polarization-maintaining (PM) optical fibers to the respective collimators where it passes a quarter-waveplate to provide the circular polarization. It is generated by two home-built narrow linewidth external cavity diode lasers [ECDL 1 and ECDL 2 in Fig. 2(a)], which operate initially at the cooling ($|F = 2\rangle \rightarrow |F' = 3\rangle$) and repumping transitions ($|F = 1\rangle \rightarrow |F' = 2\rangle$) of ^{87}Rb at 780.242 and 780.246 nm, respectively.[27] The light is amplified in two tapered amplifiers with an optical output power of up to 1 W. Subsequently, each beam passes an acousto-optic modulator that is used to control the intensities of the respective light fields. A small fraction is split off to provide light for spatially resolved absorption and fluorescence detection. The transmitted parts used for atom cooling pass an LCVR (Thorlabs LCC1111-B) and are coupled into a PM fiber-optic splitter (Evanescent Optics, 4×4 Spliceless PM Coupler Array). LCVRs consist of a transparent birefringent polymer crystal in which molecules align along the axis of the electric field generated by an applied AC voltage. Due to the adjustable level of birefringence, they act as waveplates with tunable retardance and fixed orientation. Here, they are regulated by a square-wave voltage at a frequency of 2 kHz with a variable amplitude, which allows us to continuously rotate the polarization of the incident light. The controller switches between two predefined amplitudes $V1$ and $V2$ by an external trigger. The amplitudes are chosen in order to provide two orthogonal output polarizations indicated by blue (green) arrows in Fig. 2(a), which allows us to make use of either the fast or slow polarization modes of the PM fibers. In combination with the quarter-waveplates after the fiber splitter, this enables to switch between the left- and right-circular polarizations of the MOT beams.

The switching time has been measured in an external setup to be 0.6 ms from $V1$ to $V2$ and 35 ms from $V2$ to $V1$. In principle, this time can be shortened by additional heating of the LCVRs due to the reduced viscosity of the liquid crystal polymer[28] or by using ultrafast but usually high-cost Pockels cells. Since the detection light is not affected by the LCVRs, only the fast switching direction is used during an experimental sequence. Thus, no further gain from shorter switching times is expected for the here-discussed experiments. The long-term stability of the retardance is kept below 0.02λ over more than 100 weeks,[28] which obviates any further adjustments of amplitude voltages.

This setup allows us to reverse the polarization for all beams inside the MOT when switching from the red- to the blue-detuned MOT with only two LCVRs. It additionally avoids any mechanical moving parts and is based on cost-efficient components.
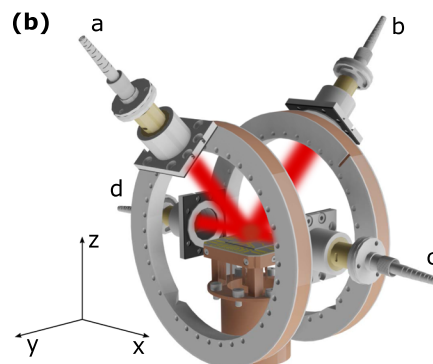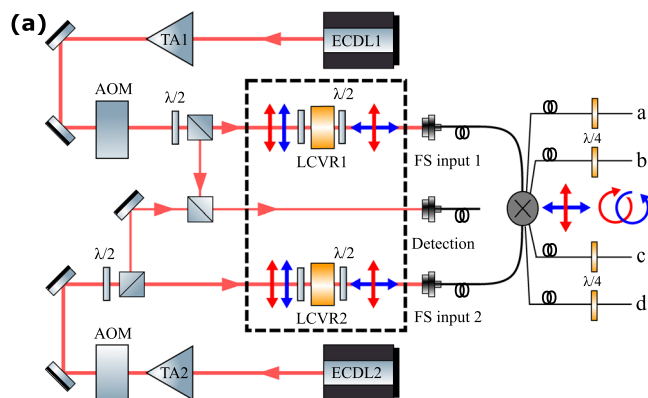

FIG. 2. (a) Setup of laser module and fiber splitter with respective fiber outputs a–d. TA: tapered amplifier, FS: fiber splitter, and AOM: acousto-optical modulator. The red (blue) arrows indicate the direction of polarization for the red- (blue-) detuned MOT. (b) Setup of the experimental chamber with the atom chip and external beam collimators. Shown are the four MOT laser beams and the atom chip. Beams a and b are reflected on the chip surface, which forms a six-beam MOT configuration.

III. EXPERIMENTS

In the following, we will discuss our measurements to determine the feasibility of a type-II MOT using the setup presented above and compare our results with the case where we only use a type-I MOT.

For the type-I MOT, the lasers ECDL 1 and 2 drive the transitions shown in Fig. 1. The cooling laser is red detuned with $\delta_{I,1} = -11$ MHz to the type-I cooling transition, the repumper is in resonance with the transition. The cooling and repumping beams operate at peak intensities of $I_{I,1} = 18.0$ mW/cm^2 and $I_{I,2} = 2.0$ mW/cm^2 for each beam at the position of the atoms, respectively. This is well above the saturation intensity $I_{sat} = 1.67$ mW/cm^2 for circularly polarized light.[27] During the type-I MOT, the LCVRs are operated with the amplitude $V1$. After the loading time T, the type-I MOT is switched off, followed by a 2 ms long period to stabilize the laser frequencies to the blue-detuned cooling transitions shown in Fig. 1. The acousto-optical modulators are switched off during this period to avoid unintended light forces on the atoms. Also, the voltages driving the LCVRs are changed to $V2$ to reverse the light polarization at the atom position. Subsequently, the lasers ECDL 1 and 2 drive the type-II transitions $|F = 2\rangle \rightarrow |F' = 2\rangle$ and $|F = 1\rangle \rightarrow |F' = 1\rangle$ with detunings of $\delta_{II,1} = 46$ MHz and $\delta_{II,2} = 22$ MHz, respectively. Notably, the "repumper" transition $|F = 1\rangle \rightarrow |F' = 1\rangle$ contributes the main part to the light forces.[15] Thus, the peak intensity of ECDL 2 is increased to its maximum value of $I_{II,2} = 8.2$ mW/cm^2, whereas the peak intensity of ECDL 1 is slightly decreased to $I_{II,1} = 13.2$ mW/cm^2 per beam. In the type-II MOT, the atoms are trapped and further cooled for 20 ms. Subsequently, the MOT light and magnetic fields are switched off and the atoms are released into free fall. With a 20-μs light pulse resonant to the transition $|F = 1\rangle \rightarrow |F' = 2\rangle$, all atoms remaining in $|F = 1\rangle$ are pumped into the cycling detection transition $|F = 2\rangle \rightarrow |F' = 3\rangle$. The atoms are detected via absorption and fluorescence imaging using the fiber output port shown in Fig. 2(a). Here, absorption imaging is primarily used for atom number detection and fluorescence imaging for expansion measurements in the x- and y-directions.

IV. RESULTS

We characterize the properties of the blue-detuned type-II MOT by determining its transfer efficiency from a type-I MOT and the achievable PSD. In Fig. 3(a), the atom number over the (type-I) MOT loading time T is shown for both MOTs in comparison. The transfer efficiency between the type-I and type-II MOT results in $(84 \pm 6)\%$ averaged overall loading times. According to simulations of the cooling forces,[16] atoms below a critical velocity of $v \approx 4.5$ m/s are expected to be trapped in the type-II MOT. Given the temperature of the type-I MOT of 1.4 mK, the transfer efficiency should be close to 100% based on a Maxwell–Boltzmann distribution of the atoms in the type-I MOT. The $1/e$-lifetime of the type-II MOT has been measured to be (512 ± 17) ms and accounts for a loss of 4% of the initially trapped atoms during the 20-ms type-II MOT period. We attribute the remaining loss fraction to atoms that escape the trapping volume of the type-II MOT during the 2 ms switching phase where the ensemble freely expands. Faster frequency jumps could, therefore, reduce these losses.

Figure 3(b) shows time-of-flight (ToF) measurements of the Gaussian ensemble width in two spatial directions σ_x and σ_y of both MOTs for a loading time of 500 ms. Here, the MOT light and the quadrupole field are switched off, allowing the ensemble to expand freely until detection. The ensemble size in the xy-plane is detected via fluorescence detection. The expansion of an ensemble containing atoms with mass m is related to its temperature via $T = m\sigma_v^2/k_B$. The parameter σ_v^2 is given by a least-squares fit of the function $\sigma^2(t) = \sigma^2(t = 0) + \sigma_v^2 t^2$. For the red-detuned type-I MOT, a geometric mean temperature of $\overline{T}_I = (1.33 \pm 0.03)$ mK is determined. In the type-II MOT, the ensemble temperature is further reduced to $\overline{T}_{II} = (44 \pm 1)\,\mu$K, which is below the Doppler temperature limit $T_D \approx 140\,\mu$K[27] and indicates efficient sub-Doppler
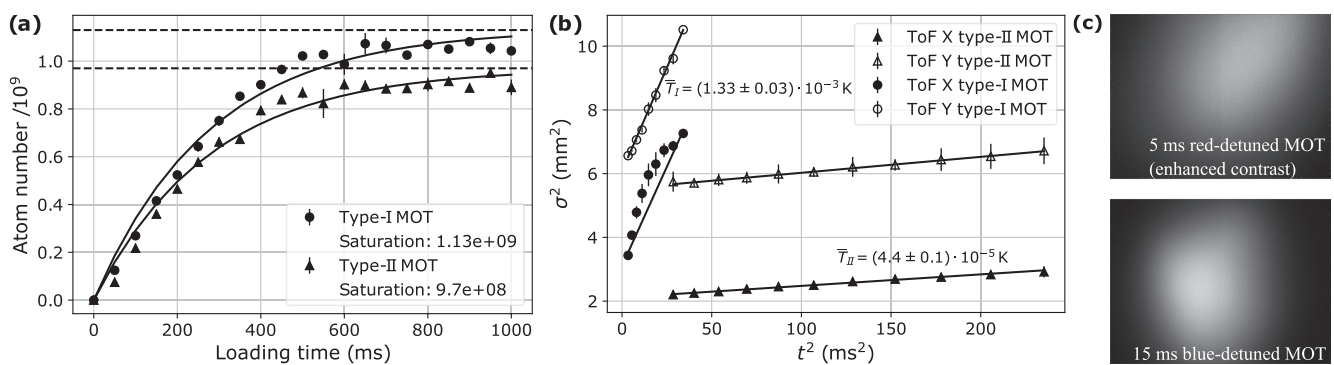
FIG. 3. (a) Comparison of atom number over loading time for both MOTs. Error bars denote the 1σ statistical uncertainty over three consecutive experimental runs. Transfer efficiency from the type-I MOT to the type-II MOT results in $(84 \pm 6)\%$. (b) Measurement of the ensemble size in the dependence of the time of flight after release from the respective MOTs in two spatial directions σ_x and σ_y (see Fig. 2 for coordinate system definition) after a loading time of 500 ms. Error bars denote three standard deviations of three consecutive experimental runs for better visibility. The parameter σ is extracted for each direction with a 1D-Gaussian fit function. The expansion is fitted with a linear model (solid lines). The type-II MOT generates lower temperatures than the type-I MOT as revealed by the lower expansion rate. (c) Fluorescence images of a red-detuned (blue-detuned) MOT after free expansions of 5 ms (15 ms). The detected image of the red-detuned MOT exceeds the size of the CCD sensor, which deforms its Gaussian envelope along the x-direction leading to the observed deviation of the type-I MOT expansion data.

cooling forces. Notably, the ensemble temperature is further reduced for smaller atom densities, which is attributed to reduced photon rescattering.[29,30] For example, a temperature of 19 μK is reached for a type-II MOT with 2.2×10^8 atoms.

The data obtained from the TOF measurement allow us to calculate the PSD of the ensemble by $\rho = n \cdot \lambda_{dB}^3$. Here, n is the initial peak density of the atom cloud right after release and

$$\lambda_{dB} = \sqrt{\frac{2\pi\hbar^2}{mk_BT}}$$

denotes the thermal de Broglie wavelength. The peak density is evaluated using $n = N/((\sqrt{2\pi})^3 \sigma_x \sigma_y \sigma_z)$ with the total atom number N and the initial Gaussian widths $\sigma_{x,y,z}$ immediately after release. Here, the z-direction is accessible via absorption detection.

These equations lead to densities and PSDs of the ensembles after the type-I MOT (n_I, ρ_I) and after the type-II MOT (n_II, ρ_II) of

$$n_\mathrm{I} = (6.8 \pm 0.2) \cdot 10^9 \text{ cm}^{-3},$$
$$\rho_\mathrm{I} = (9.2 \pm 0.4) \cdot 10^{-10},$$
$$n_\mathrm{II} = (1.2 \pm 0.1) \cdot 10^{10} \text{ cm}^{-3},$$
$$\rho_\mathrm{II} = (2.7 \pm 0.1) \cdot 10^{-7}.$$

The PSD of the type-II MOT exceeds that of the type-I MOT by more than two orders of magnitude.

The setup also provides an atom source and the laser system for cooling and manipulation of ^{41}K and ^{39}K, which have the most spectroscopic features of ^{87}Rb in common.[31] In contrast to ^{87}Rb, they exhibit narrow hyperfine splittings of D2 transitions, which complicates laser cooling of ^{41}K and ^{39}K in standard type-I MOTs.[32,33]

By adopting the above-described changes in the potassium laser system, the feasibility of a blue-detuned type-II MOT for cooling of ^{41}K and ^{39}K is explored. For both isotopes, cooling and trapping are only achieved if solely the polarization of the blue-detuned repumping light field is reversed. The cooling laser remains in the red-detuned type-I configuration. The experiments show neither higher densities nor lower temperatures for the mixed type-I/II MOT, indicating no advantages compared to the pure type-I MOT. This is attributed to additional heating due to simultaneously driven type-I transitions within the narrow level splitting of potassium.

V. CONCLUSION

The setup and measurements presented in this paper demonstrate the feasibility of a blue-detuned type-II MOT by utilizing LCVRs for the fast polarization control. This allows for a low-cost implementation in existing experimental setups without the need for additional lasers or beam collimators.

By switching from the red-detuned type-I to the blue-detuned type-II transitions with the reversed polarization, 85% of the ^{87}Rb atoms trapped in the type-I MOT were transferred into the type-II MOT. TOF measurements show that a geometric mean temperature of $\overline{T}_\mathrm{II} = 44\ \mu$K was reached. This is well below the Doppler temperature $T_D \approx 140\ \mu$K, which typically constitutes the lower temperature

limit within a type-I MOT. Furthermore, the PSD of the type-II MOT is shown to be increased by more than two orders of magnitude compared to the type-I MOT. Among other methods such as dark spontaneous-force MOTs,[9,10] blue-detuned type-II MOTs offer an alternative and easy-to-implement route to effectively increase the PSD of trapped ensembles.

A type-II MOT combines the advantages of sub-Doppler cooled optical molasses with the convenient position control of a trapped ensemble. Hence, type-II MOTs might also help to improve the mode matching between the MOT and consecutive stages of trapping and cooling, in particular for magnetic or optical dipole traps. Accordingly, center-of-mass oscillations of transferred ensembles due to positional mismatch could be reduced to a minimum compared to free-falling optical molasses.

LCVRs prove to be simple and compact devices to efficiently improve the atom cooling performance. This applies especially for setups with rigorous constraints on space, power consumption, and weight like experiments on mobile[20,21] or microgravity platforms.[22–24]

AUTHOR DECLARATIONS

Conflict of Interest

The authors have no conflicts to disclose.

DATA AVAILABILITY

The data that support the findings of this study are available from the corresponding author upon reasonable request.

REFERENCES

[1] R. Geiger, A. Landragin, S. Merlet, and F. Pereira Dos Santos, "High-accuracy inertial measurements with cold-atom sensors," AVS Quantum Sci. **2**, 024702 (2020).

[2] A. D. Ludlow, M. M. Boyd, J. Ye, E. Peik, and P. O. Schmidt, "Optical atom clocks," Rev. Mod. Phys. **87**, 637–701 (2015).

[3] Z.-T. Lu and P. Mueller, "Atom trap trace analysis of rare noble gas isotopes," Adv. At., Mol., Opt. Phys. **58**, 173–205 (2010).

[4] A. V. Steele, A. Schwarzkopf, J. J. McClelland, and B. Knuffman, "High-brightness Cs focused ion beam from a cold-atomic-beam ion source," Nano Futures **1**, 015005 (2017).

[5] W. D. Phillips, "Nobel lecture: Laser cooling and trapping of neutral atoms," Rev. Mod. Phys. **70**, 721 (1998).

[6] M. Prentiss, A. Cable, J. E. Bjorkholm, S. Chu, E. L. Raab, and D. E. Pritchard, "Atomic-density-dependent losses in an optical trap," Opt. Lett. **13**, 452–454 (1988).

[7]T. Walker, D. Sesko, and C. Wieman, "Collective behavior of optically trapped neutral atoms," Phys. Rev. Lett. **64**, 408 (1990).

[8]M. Walhout, J. Dalibard, S. L. Rolston, and W. D. Phillips, "$\sigma_+-\sigma_-$ Optical molasses in a longitudinal magnetic field," J. Opt. Soc. Am. B **9**, 1997–2007 (1992).

[9]W. Ketterle, K. B. Davis, M. A. Joffe, A. Martin, and D. E. Pritchard, "High densities of cold atoms in a dark spontaneous force optical trap," Phys. Rev. Lett. **70**, 2253 (1993).

[10]N. Radwell, G. Walker, and S. Franke-Arnold, "Cold-atom densities of more than 10^{12} cm^{-3} in a holographically shaped dark spontaneous-force optical trap," Phys. Rev. A **88**, 043409 (2013).

[11]B. K. Stuhl, B. C. Sawyer, D. Wang, and J. Ye, "Magneto-optical trap for polar molecules," Phys. Rev. Lett. **101**, 243002 (2008).

[12]J. F. Barry, D. J. McCarron, E. B. Norrgard, M. H. Steinecker, and D. DeMille, "Magneto-optical trapping of a diatomic molecule," Nature **512**, 286–289 (2014).

[13]M. R. Tarbutt and T. C. Steimle, "Modeling magneto-optical trapping of CaF molecules," Phys. Rev. A **92**, 053401 (2015).

[14]S. Truppe, H. Williams, M. Hambach, L. Caldwell, N. Fitch, E. Hilds, B. Sauer, and M. Tarbutt, "Molecules cooled below the Doppler limit," Nat. Phys. **13**, 1173–1176 (2017).

[15]J. A. Devlin and M. R. Tarbutt, "Three-dimensional Doppler, polarization-gradient, and magneto-optical forces for atoms and molecules with dark states," New J. Phys. **18**, 123017 (2016).

[16]K. N. Jarvis, J. A. Devlin, T. E. Wall, B. E. Sauer, and M. R. Tarbutt, "Blue-detuned magneto-optical trap," Phys. Rev. Lett. **120**, 083201 (2018).

[17]D. B. Tretyakov, I. I. Beterov, V. M. Entin, I. I. Ryabtsev, and P. L. Chapovsky, "Investigation of cold rubidium Rydberg atoms in a magneto-optical trap," J. Exp. Theor. Phys. **108**, 374–383 (2008).

[18]J. Han, Y. Jamil, D. V. L. Norum, P. J. Tanner, and T. F. Gallagher, "Rb *nf* quantum defects from millimeter-wave spectroscopy of cold ^{85}Rb Rydberg atoms," Phys. Rev. A **74**, 054502 (2006).

[19]K. Afrousheh, P. Bohlouli-Zanjani, J. D. Carter, A. Mugford, and J. D. D. Martin, "Resonant electric dipole-dipole interactions between cold Rydberg atoms in a magnetic field," Phys. Rev. A **73**, 063403 (2006).

[20]A. Hinton, M. Perea-Ortiz, J. Winch, J. Briggs, S. Freer, D. Moustoukas, S. Powell-Gill, C. Squire, A. Lamb, C. Rammeloo, B. Stray, G. Voulazeris, L. Zhu, A. Kaushik, Y.-H. Lien, A. Niggebaum, A. Rodgers, A. Stabrawa, D. Boddice, S. R. Plant, G. W. Tuckwell, K. Bongs, N. Metje, and M. Holynski, "A portable magneto-optical trap with prospects for atom interferometry in civil engineering," Philos. Trans. R. Soc. **375**, 20160238 (2017).

[21]Y. Bidel, N. Zahzam, C. Blanchard, A. Bonnin, M. Cadoret, A. Bresson, D. Rouxel, and M. F. Lequentrec-Lalancette, "Absolute marine gravimetry with matter-wave interferometry," Nat. Commun. **9**, 627 (2018).

[22]J. Rudolph, W. Herr, C. Grzeschik, T. Sternke, A. Grote, M. Popp, D. Becker, H. Müntinga, H. Ahlers, A. Peters, C. Lämmerzahl, K. Sengstock, N. Gaaloul, W. Ertmer, and E. M. Rasel, "A high-flux BEC source for mobile atom interferometers," New J. Phys. **17**, 065001 (2015).

[23]B. Piest, "Bose-Einstein condensation of K-41 and Rb-87 on an atom chip for sounding rocket missions" Doctoral Dissertation, Gottfried Wilhelm Leibniz Universität Hannover, 2021.

[24]K. Frye, S. Abend, W. Bartosch, A. Bawamia, D. Becker, H. Blume, C. Braxmaier, S.-W. Chiow, M. A. Efremov, W. Ertmer, P. Fierlinger, T. Franz, N. Gaaloul, J. Grosse, C. Grzeschik, O. Hellmig, V. A. Henderson, W. Herr, U. Israelsson, J. Kohel, M. Krutzik, C. Kürbis, C. Lämmerzahl, M. List, D. Lüdtke, N. Lundblad, J. P. Marburger, M. Meister, M. Mihm, H. Müller, H. Müntinga, A. M. Nepal, T. Oberschulte, A. Papakonstantinou, J. Perovšek, A. Peters, A. Prat, E. M. Rasel, A. Roura, M. Sbroscia, W. P. Schleich, C. Schubert, S. T. Seidel, J. Sommer, C. Spindeldreier, D. Stamper-Kurn, B. K. Stuhl, M. Warner, T. Wendrich, A. Wenzlawski, A. Wicht, P. Windpassinger, N. Yu, and L. Wörner, "The Bose-Einstein condensate and cold atom laboratory," EPJ Quantum Technol. **8**, 1 (2021).

[25]R. Folman, P. Krüger, D. Cassettari, B. Hessmo, T. Maier, and J. Schmiedmayer, "Controlling cold atoms using nanofabricated surfaces: Atom chips," Phys. Rev. Lett. **84**, 4749 (2000).

[26]S. Wildermuth, P. Krüger, C. Becker, M. Brajdic, S. Haupt, A. Kasper, R. Folman, and J. Schmiedmayer, "Optimized magneto-optical trap for experiments with ultracold atoms near surfaces," Phys. Rev. A **69**, 030901 (2004).

[27]D. A. Steck, "Rubidium 87 D line data," https://steck.us/alkalidata/rubidium87numbers.1.6.pdf (2001, revised 2003).

[28]Datasheet LCC1111-B, Thorlabs, http://www.thorlabs.com.

[29]G. Hillenbrand, C. J. Foot, and K. Burnett, "Heating due to long-range photon exchange interactions between cold atoms," Phys. Rev. A **50**, 1479 (1994).

[30]C. G. Townsend, N. H. Edwards, C. J. Cooper, K. P. Zetie, C. J. Foot, A. M. Steane, P. Szriftgiser, H. Perrin, and J. Dalibard, "Phase-space density in the magneto-optical trap," Phys. Rev. A **52**, 1423 (1995).

[31]T. G. Tiecke, "Properties of potassium," https://www.tobiastiecke.nl/archive/PotassiumProperties.pdf (2019).

[32]R. S. Williamson and T. Walker, "Magneto-optical trapping and ultracold collisions of potassium atoms," J. Opt. Soc. Am. B **12**, 1393–1397 (1995).

[33]M. Prevedelli, F. S. Cataliotti, E. A. Cornell, J. R. Ensher, C. Fort, L. Ricci, G. M. Tino, and M. Inguscio, "Trapping and cooling of potassium isotopes in a double-magneto-optical-trap apparatus," Phys. Rev. A **59**, 886 (1998).